Journal of
Marine Science and Engineering

MDPI

Article

Effects of Floating Airbag on Cable Hydrodynamic Behaviors: An Experimental Study

Shanjun Bao [1], Zhigang Zhang [1], Zhoulong Yuan [1], Jiancheng Wang [1], Qianhao Yu [1] and Zhen Liu [2,*]

[1] Submarine Power Cable Engineering Company, Zhejiang Qiming Electric Power Group Co., Ltd., Zhoushan 316000, China; bsj663311@163.com (S.B.); zsxm2018@126.com (Z.Z.); 13868209580@163.com (Z.Y.); wjc8825@126.com (J.W.); yuqianhao665219@126.com (Q.Y.)
[2] Shandong Provincial Key Laboratory of Ocean Engineering, Ocean University of China, Qingdao 266100, China
* Correspondence: liuzhen@ouc.edu.cn

Abstract: The development of an offshore island presented a need to construct an electricity grid with the laying of submarine cable. The floating airbag is a useful tool for cable construction, especially during landing. The effects of these airbags on cable hydrodynamic behaviors were investigated in this study. Regular wave conditions with various airbag intervals and cable masses were employed in wave flume tests. The vertical displacements and tensions of the cable under different test conditions were investigated. It was found that the peak values of the displacement amplitudes and tensions were obtained during the cable landing phase.

Keywords: cable landing; floating airbag; hydrodynamic behaviors; experimental study

check for updates

Citation: Bao, S.; Zhang, Z.; Yuan, Z.; Wang, J.; Yu, Q.; Liu, Z. Effects of Floating Airbag on Cable Hydrodynamic Behaviors: An Experimental Study. *J. Mar. Sci. Eng.* **2022**, *10*, 402. https://doi.org/10.3390/jmse10030402

Academic Editors: Pasqualino Corigliano and Vincenzo Piscopo

Received: 5 February 2022
Accepted: 6 March 2022
Published: 10 March 2022

1. Introduction

In recent decades, the demands for marine electricity transformation have increased because of the rapid increase in the development of offshore electrical systems and offshore renewable energy. These demands can be satisfied by connecting these offshore electrical units to the mainland grid using submarine cables [1–3]. The construction difficulty and safety demands are both higher during the cable landing phase than during other processes [4]. Floating assistant facilities can be used to prevent possible friction with the seabed and reduce the pull forces [5], which increases the safety of the cable landing. Therefore, study of the tensions and hydrodynamic forces on the cable during its landing with floating assistant facilities is needed to guarantee the engineering quality and increase the construction efficiency in the construction of submarine cables.

The tensions and hydrodynamic forces on the cable during its laying have been investigated comprehensively based on various assumptions. Zajac first proposed the steady-state theory [6], which assumes the cable to be a straight line and excluded all effects from transient motion. It now appears that unsteady-state theory is more suitable for this analysis. Huang reported a new methodology to predict the three-dimensional (3D) dynamic motions of a submarine cable [7]. Vaz and Patel considered external water loads and proposed a two-dimensional (2D) predictive model of cable transient characteristics [8], and a further 3D model for the investigation of cable transient behaviors during cable laying [9]. Furthermore, the 3D dynamic characteristics of a cable in different sea currents were studied [10]. Hover et al. simplified the flexible cable as a series of interconnected straight-line sections without any consideration of bending moments and simulated the motions of the submarine cable dynamically [11]. Based on linear and nonlinear methods, Wang et al. established a dynamic model for a submarine, derived its governing equations, and analyzed the effects of vessel speed, water depth, and length on cable safety [12]. Park et al. studied the dynamic behaviors of a submarine cable using both experimental and numerical methods [13]. Cao et al. proposed a dynamic differential equation of the cable laying process considering the bending stiffness, which was employed in an investigation of the effects of bending stiffness, vessel motion, the incident angle of the cable, and the seabed stiffness on the tensions and motions of the cable [14]. Jasman et al. analyzed the tensions of various types of submarine cables using a 2D numerical model [15]. Mamatsopoulos et al. developed a numerical tool to compute the safety coefficient of a submarine cable during laying operations [16].

During laying operations, tension variations caused by external loads such as the wind, current, waves, and the laying vessel motions are inevitable. Nagatomi et al. applied the concentrated mass method (CMM) to calculate the motions and tensions of a submarine cable [17], and compared the calculations with field test results. Prpić-Oršić et al. [18] proposed a time-domain model for prediction of the tensions and motions of a cable-laying process. Yang et al. investigated the effects of sea currents, vessel motion, and water depth on cable tensions [19]. Feng et al. established a 3D finite-element cable model and studied the dynamic characteristics of a cable in ocean waves [20]. Ye et al. established a kinematic formula to calculate the overall cable motions during a laying operation [21]. Based on some simplifications, Zhang et al. [22] analyzed the dynamic characteristics of a cable as it was laid on the seabed using CMM, and validated these results with experimental data.

Despite the literature reviewed above, the coupled influence of the cable and typical floaters during the landing process has been little explored in the literature. In addition, floating assistant facilities are being utilized more and more in engineering applications, and their hydrodynamics when coupled with a landing submarine cable should be investigated to provide more information and guidance to these field operations. In this study, an experimental study on the hydrodynamic forces on a landing cable with typical floaters was conducted, and the kinematic and dynamic characteristics of the cable were analyzed.

2. Floating Airbags for Cable Landing

During the cable landing process, a pulling rope with one end connected to the cable head is fixed to an onshore winch at the other end. As the winch operates, the rope with the cable is pulled from the vessel head to the shore. If there are no floaters with the cable, it will sink underwater to different depths because of the cable's weight. The sinking of the cable increases the tension and friction during the pulling. If additional floaters are attached to the cable at consistent intervals, the cable will float on the sea surface and can easily be pulled to the shore, as shown in Figure 1. In China, waste tires are employed as floating supporters to provide additional buoyancy, which are easy to install and hard to remove once the cable is in position.

To improve the cable landing capability and the degree of construction automation, the Zhejiang Qiming Electric Power Group Co., Ltd. cooperated with the Trelleborg Ocean Engineering Company and the Ocean University of China to develop a new, reusable floating airbag especially for cable landing construction, as shown in Figure 2. The prototype floater has a length of 1.0 m and a width of 0.7 m, and contains two chambers for air charging. When the two chambers are fully submerged, a floater is able to provide a buoyancy of 0.2 tons.

The airbag consists of two pillows connected side by side, which can be filled rapidly with gas according to the pressure and buoyancy demands on the vessel head, and can be bound to the cable artificially. The band holding the airbags around the cable uses an auto-lock catch. The cable is pulled into the water with one airbags at a time. Once the cable is in the correct position following the shallow water part of the process, the airbags are separated from the cable by releasing the auto-lock bands in a predetermined sequence using remote control. The assembled cable and the cable with released airbags are schematically illustrated in Figure 3. Subsequently, the cable can sink down to the seabed. The airbags are linked with a guidance line connected to an onshore winch, and can be pulled to the shore for recycling. The automatic lock and release of the prototype-sized airbags were tested and verified in a wave tank, as shown in Figure 4.

Figure 1. Floating airbags used in engineering. Reproduced from ref. [23]; copyright (2017) with permission from Nexans.

Figure 2. Floating airbag (prototype size).

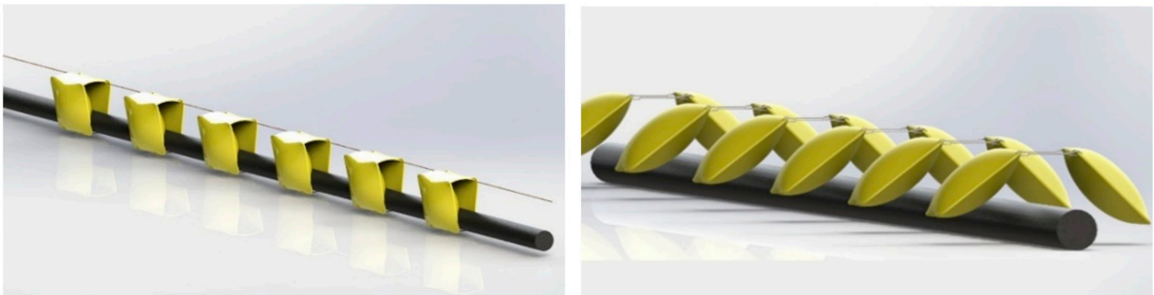

(a) (b)

Figure 3. Two critical design statuses of the airbags: (a) locked status, (b) released status.

(a) (b)

Figure 4. Experimental verification of the airbag lock and release in the tank: (a) locked status, (b) released status.

3. Experimental Setup

All the experiments were conducted in the wave-current flume of the hydrodynamic laboratory at Shandong Provincial Key Laboratory of Ocean Engineering, Ocean University of China. The length and width of the flume are 30 m and 0.6 m, respectively. The maximum operating depth is 0.6 m. A wavemaker is installed at one end of the flume, and can be controlled to generate desired regular and irregular wave scenarios.

As waves are regarded as the dominant environmental factor in shallow water, we employed only waves in all experimental cases in this study. The effects of the coastal current on the lateral movement of the cable will be investigated in the future. The motion and hydrodynamic responses caused by the external loads such as wind, current, and laying vessel will be investigated in subsequent studies. With regard to high-frequency responses like mechanical vibrations, the lower-frequency displacement of the cable was the main focus of our research. Considering the laboratory and natural conditions, we set the scale ratio as λ_l = 1:18, following the Froude similarity criterion.

The typical engineering area considered is around Zhoushan Islands, where the bathymetry is plane and the seabed slope is less than 2°. Considering the flume length, we set the seabed slope in the experimental study as 2°. Considering the natural bathymetry in Zhoushan and the testing conditions of the experimental flume, the scale ratio was fixed as 1:18 based on the Froude similarity criterion. The slope was designed and manufactured using a steel frame and rough planks to simulate the actual seabed in these shallow waters. A detailed design illustration and a physical photo of the slope in the flume are provided in Figure 5.

Submarine cables are hard to model in experimental studies because their cross-sections can vary among cables for different purposes, which causes the mass per unit length and elasticity modulus to vary as well. Several typical submarine cables were chosen for model selection, and mass per unit length was employed as the criterion. By equilibrating the mass and the elasticity modulus to be close to the actual values under the preset scale ratio, three typical model cables were fixed: 0.26 kg/m, 0.34 kg/m, and 0.44 kg/m. The diameters of the cable cross-sections were 10.5 mm, 12.5 mm, and 15 mm, respectively. The airbag models were custom-ordered from the factory, following the similarity criterion to determine the size, the material, and the inflatable volume. The material was polyethylene (PE). The inflation volume of each side of an airbag was 34 cm^3, with airbags being 56 mm long and 38 mm wide. The model airbag and cables are presented in Figure 6; these were produced using the scale ratio to determine the size and air-charging volume.

During the experiments, the free surface elevation was measured by capacitor wave gauges. The vertical displacement of the cable at specific points was recorded by a draw-string type displacement sensor, as shown in Figure 7. The variation of the tension in the model cable was measured at both ends by a tension transducer, as shown in Figure 8.

In the experiments, the maximum water depth without any slope was fixed at 0.3 m. The wave scenarios only applied regular wave conditions for better identification of the hydrodynamic behaviors of the cable and airbags, which will be beneficial to understanding the complicated responses under irregular wave conditions in future studies. For the regular wave conditions, the wave heights H_R were 0.05 m and 0.1, and the wave period T_R varied from 1.5 s, 1.75 s, to 2.0 s. Therefore, six regular wave scenarios were employed.

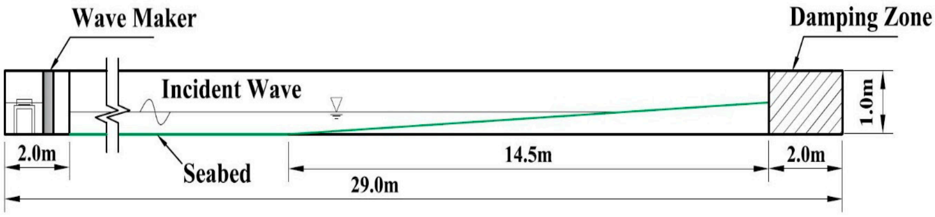

(**a**)

(**b**)

Figure 5. Seabed slope model: (**a**) designed seabed slope in the wave flume, (**b**) physical photo of the seabed slope model.

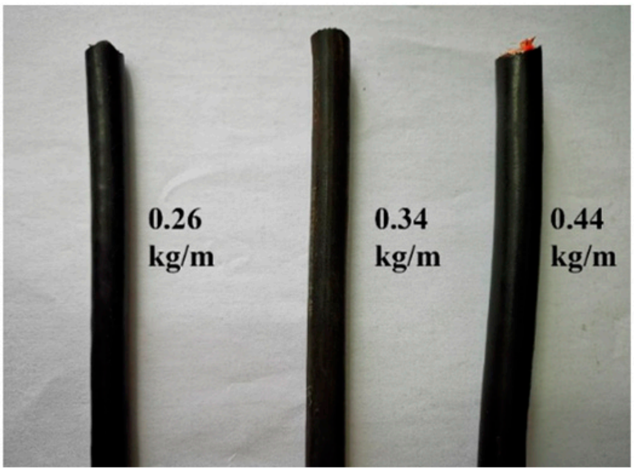

(**a**)

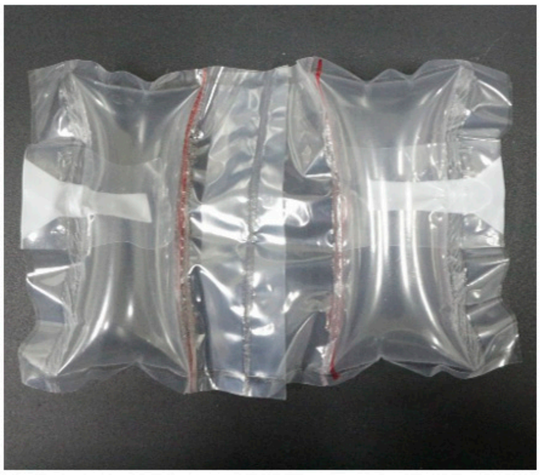

(**b**)

(**c**)

Figure 6. Model airbag and cables used in the experimental study: (**a**) model cables, (**b**) model airbag, (**c**) model cable bounded with airbags.

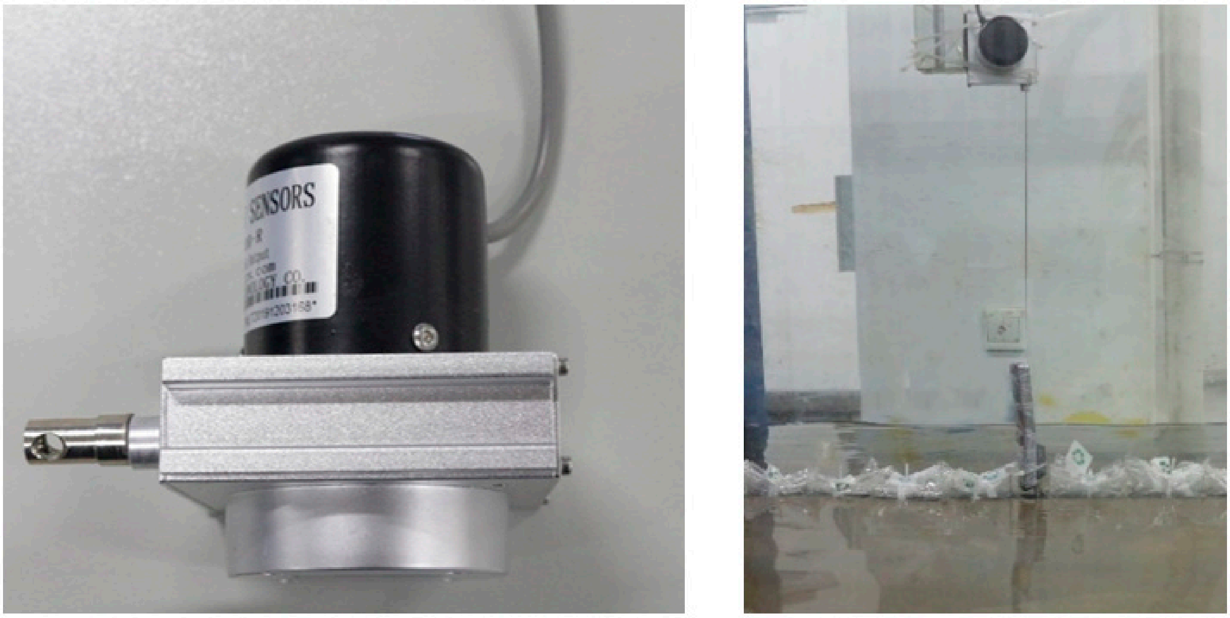

Figure 7. Drawstring displacement sensor.

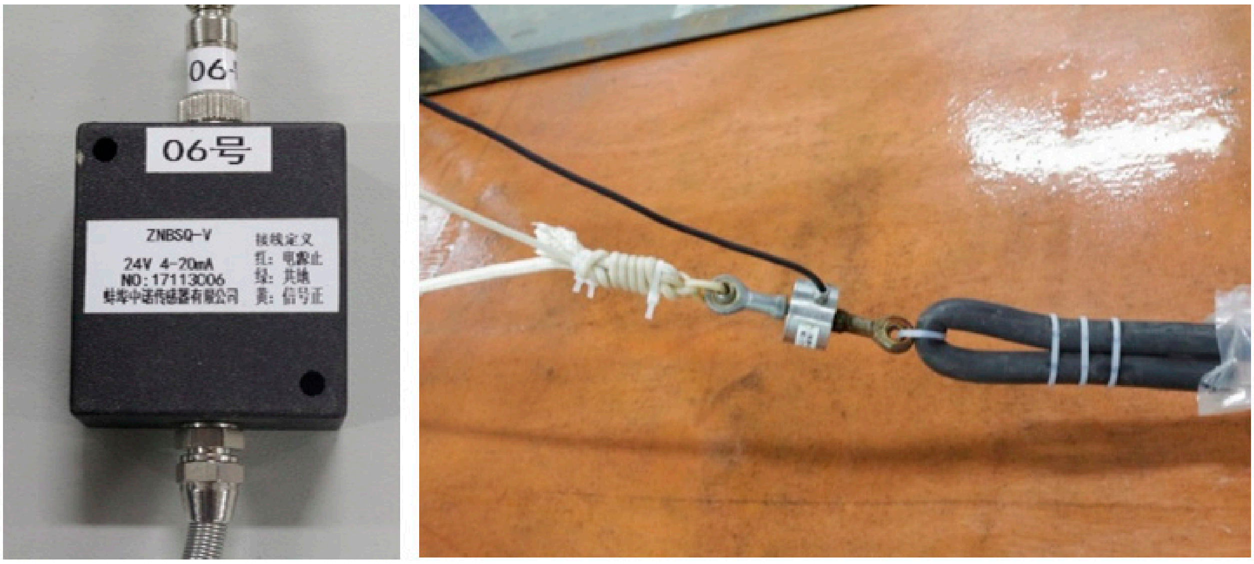

Figure 8. Tension transducer. (Text description: Made in Bengbu chino sensor Co., Ltd, Bengbu, China; Wiring definition (red: Power+; green: common-ground; yellow: Signal+)).

To understand the dynamic behaviors of the cable bound with airbags, as shown in Figure 9, four typical lengths of the cable L_S were tested in the water to represent different phases of the cable during its landing process. L_S = 4.0 m, L_S = 6.0 m, L_S = 10.0 m, and L_S = 16.0 m represent the initial, intermediate, landing, and ending phases, respectively. L_W represents the distance between the two ends in the flume, which was 25.0 m. The interval between the displacement sensors L_I increase as L_S increased. For the last three phases, there were four sensors, and the values of L_I were 1.4 m, 2.0 m, and 2.4 m, respectively. For the initial phase, as the cable length in the water was short, only three sensors were used and L_I = 1.0 m. The intervals between the airbags were different for various masses of the cable, as listed in Table 1. All the measured data were processed by the data acquisition (DAQ) system developed by the research team, with the instrumental chain shown in Figure 10. During the test, data were recorded at least every 60s; meanwhile, stable cycles of 10 regular waves were used to evaluate key parameters. It is worth mentioning is that in the actual construction process, the pulling rope play a role in floating airbag recycling and storage projects. In the experimental tests, the rear end of the submarine cable was connected with the tension sensor and the pulling rope was only used to adjust the length of the cable in the four stages in still water. There was no buoyant force here because the pulling rope did not come into contact with the water. The total number of cases was 216 in this study. For the regular wave scenarios, fewer than 12 waves were generated for test and recording. All the cases were repeated three times to compute the average values of each case.

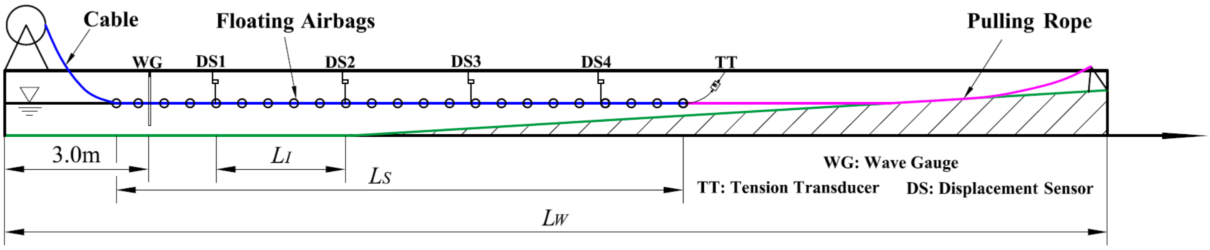

Figure 9. Deployment of the model cable and airbags with the instruments.

Table 1. Airbag intervals for model cables with different masses.

Mass per Length of the Cable G (kg/m)	Constant Intervals between Airbags I_A (cm)
0.26	14.0
	17.0
	20.0
0.34	11.0
	13.0
	15.0
0.44	7.8
	9.8
	11.8

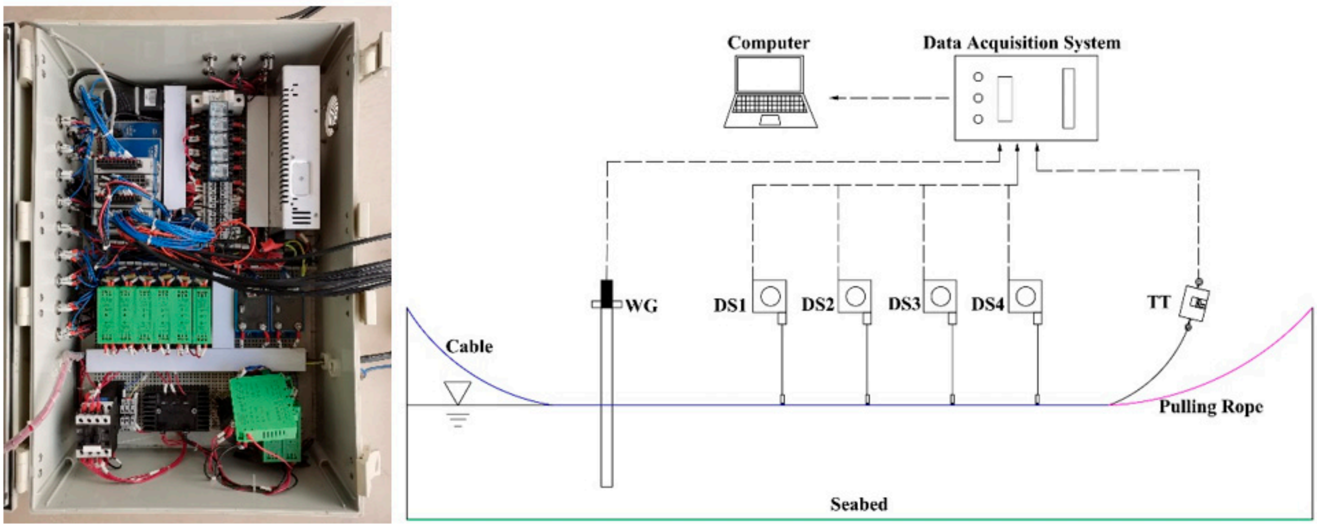

Figure 10. DAQ system and instrumental chain.

4. Results and Discussion

4.1. Typical Time Histories of the Tension and Vertical Displacements

The following conditions were chosen as a typical experimental case: G = 0.34 kg/m, H_R = 0.05 m, T_R = 1.5 s in the ending phase. The distances of the four displacement sensors DS-1, DS-2, DS-3, and DS-4 from the wavemaker were 2.5 m, 4.9 m, 7.3 m, and 9.7 m, respectively. The time histories of the vertical displacements for the cable at these positions are shown in Figure 11, where the transient vertical displacement away from the free surface is defined as a_c and the incident wave amplitude as A, with the transient relative vertical displacement as a_c/A. In addition, a_I is the instantaneous free-surface elevation and the relative elevation can be defined as a_I/A.

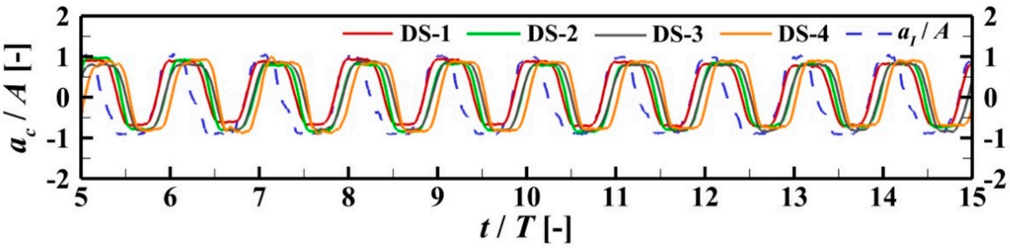

Figure 11. Time histories of incident wave elevation and the vertical displacements of the cable.

The periods of vertical oscillation at different positions were the same. As the position varied from DS-1 to DS-4, the value of the vertical displacement amplitude increased from 0.82, 0.85, and 0.94 to 0.96. The motion amplitudes of the cable at different positions were all less than those of the free surface elevation, which were caused by the cable stiffness. During the surface ascending, the cable was restricted by its weight and stiffness, with limited uplifting amplitudes. Meanwhile, the cable was observed to suspend at the extreme position during its ascending and descending with a period of approximately 0.25 T_R because of the incident waves and effects of the displacement sensors. Therefore, trapezoidal varying shapes could be found for the time-history curves for the relative motions of the cable. On the other hand, during the surface descending, compared to the wave amplitude, the cable stiffness also resulted in a smaller falling amplitude. Additionally, it was observed that the cable halted at the peaks and valleys during its oscillation at all displacement measuring points, where the halting period was 0.25 T_R. Consequently, the relative oscillating profiles all showed a similar trapezoidal shape.

A phase difference was observed between the adjacent sensors, which was 1/25 of the incident period. The ratio between the sensor interval and incident wavelength was also 1/25, indicating that the phase difference was mainly determined by the distances between the sensors. As the sensor position approached the beach, the relative vertical displacement increased because of shallow water effects and the reduction of cable stiffness caused by the connection with the pulling rope.

During the cable landing, the tension in the cable was affected by the incident wave height and period, the cable mass, and the interval between airbags. The nondimensional tension in the cable f_I can be defined as follows:

$$f_I = \frac{FT_R^2}{GH_R I_A} \tag{1}$$

where, F is the measured tension in the cable, G is the coefficient related to the mass per length of the cable, and I_A is the distance between two floating airbags. The time history of the nondimensional tension variation in the cable is illustrated in Figure 12. The variation curve shape of the tension was quasisinusoidal. Its varying period was equal to the incident wave period T_R. The peak, valley, and average values of f_I were 9.7×10^3, 8.9×10^3, and 9.3×10^3, respectively.

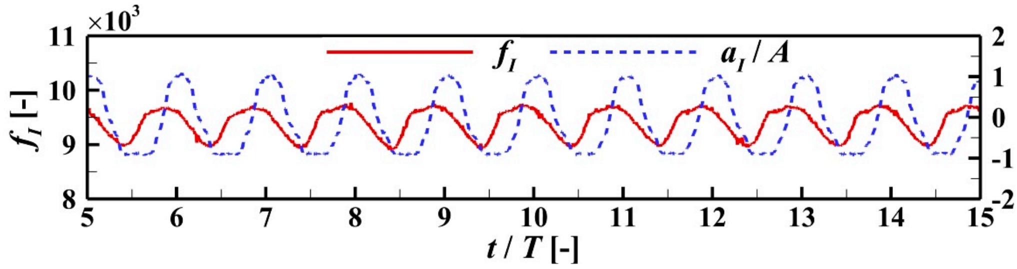

Figure 12. Time history of tension in the model cable.

Based on the statistical analysis of this case (G = 0.34 kg/m, H_R = 0.05 m, T_R= 1.5 s), Figure 13 illustrates the configuration of means and error bars of the standard deviation for the values measured by the DS (Displacement Sensors) and TT (Tension Transducer). The vertical displacement, maximum tension, and variation coefficient of means (defined as the ratio between standard deviation and average) were 2.8%, 2.7%, and 3.1%, respectively. These results show the good accuracy and repeatability of the present study.

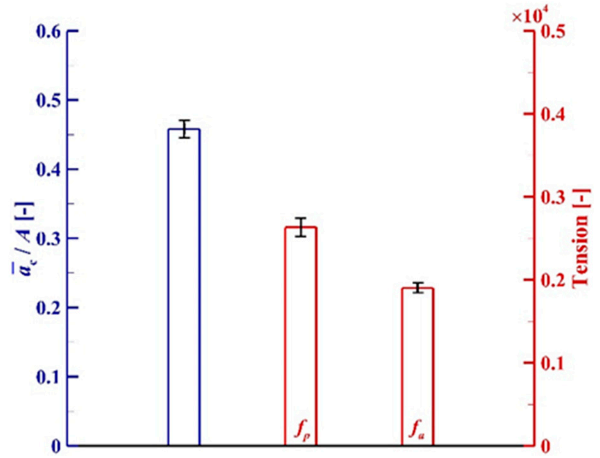

Figure 13. Error bars of one standard deviation for the measured values.

4.2. Effects of Airbag Interval on Cable Vertical Displacements

During cable landing, the vertical displacement of the cable is mainly affected by the incident wave conditions and the buoyancy provided by the airbags, which is determined by the number and intervals of the airbags. Generally, more airbags with a smaller interval can provide greater buoyancy to avoid overturning with higher stability. On the other hand, more airbags increases the construction costs and creates difficulties for the operators in installing the airbags on the cable efficiently. It is valuable to investigate the effects of airbag intervals on vertical cable displacement, which will provide more information for airbag design.

Figure 14 presents the relative vertical displacements of the cable under the condition of H_R = 0.05 m and G = 0.34 kg/m, where $\overline{a_c}$ and λ represent the average amplitude of the vertical displacements derived from various sensors and the incident wavelength, respectively. L_W is the distance from the cable landing vessel to the winch on the shore, which was 25.0 m in the experiments. For H_R = 0.05 m, all the relative displacement amplitudes were less than 1.0, which indicates that the vertical motion amplitude of the cable was less than that of the incident waves. In addition, the cable landing phases (L_S/L_W = 0.4) had significant effects on vertical displacement. As the cable head approached the shore, the vertical displacement first increased and then decreased. The peak values were obtained during the landing phase, to which more attention should be paid in practical engineering. Generally, the vertical displacement decreased as the value of I_A/λ increased, which was caused by the increase in the interval and the corresponding decrease in the buoyancy. Consequently, it was harder for the cable to oscillate vertically under the influence of waves.

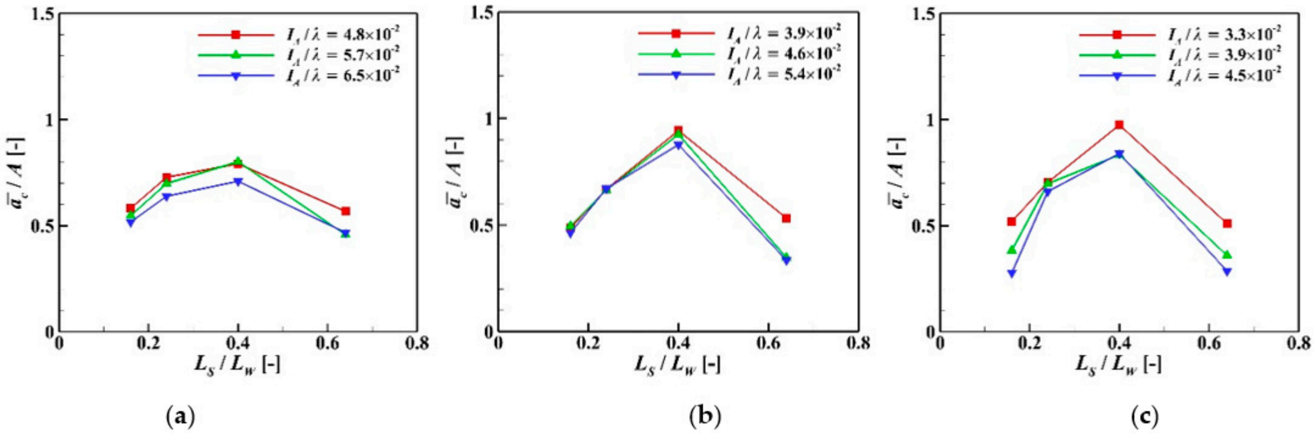

Figure 14. Effects of the airbag interval on the vertical displacement of the cable (H_R = 0.05 m): (**a**) T_R = 1.5 s, (**b**) T_R = 1.75 s, (**c**) T_R = 2.0 s.

The effects of the airbag intervals on the vertical displacement of the cable under a wave height of H_R = 0.1 m are illustrated in Figure 15. Compared to the smaller wave height of H_R = 0.05 m, the operation phase had fewer effects on the vertical displacement, especially for the first three phases, and the peak values were also obtained at the landing phase. The effects of the airbag interval on the vertical displacement were similar to those observed for H_R = 0.05 m. The maximum vertical displacement of submarine cable occurred in the stage of cable landing. The reason is that with increasing length, the influence of cable flexibility on displacement response decreased gradually, and the influence of the waves became the main factor. The significant decrease in displacement at the ending phase was due to the fact that the rear end of the cable was in contact with the seabed. Furthermore, the vertical displacement amplitude decreased as the incident wave period increased. The above results indicate that a reasonable interval between airbags should be chosen according to the local wave conditions.

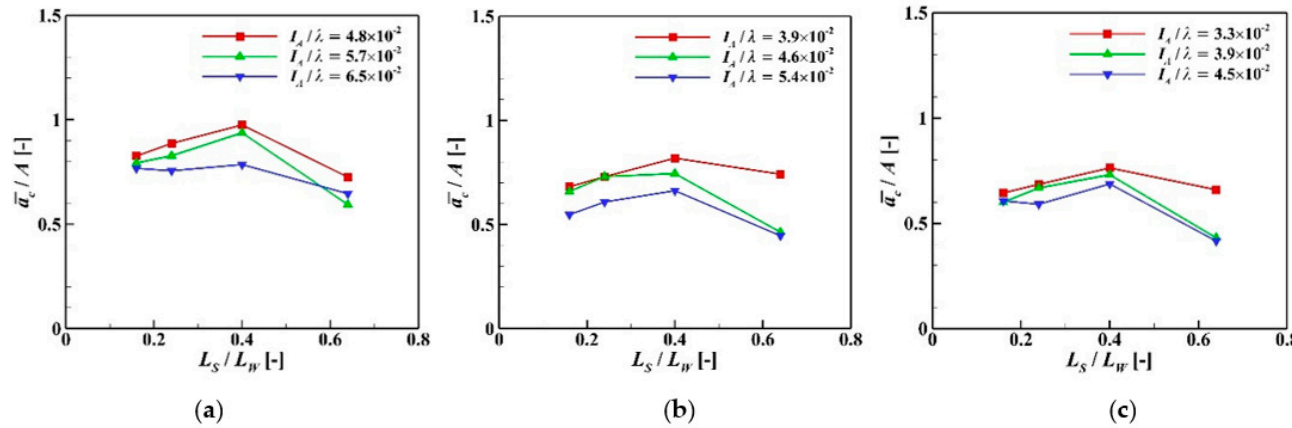

Figure 15. Effects of the airbag interval on the vertical displacement of the cable (H_R = 0.1 m): (**a**) T_R = 1.5 s, (**b**) T_R = 1.75 s, (**c**) T_R = 2.0 s.

4.3. Effects of Airbag Interval on Cable Tension

For a better understanding of the comprehensive effects of airbag interval on the cable tension, the average and peak values of the tension are summarized in this section. The average and peak tensions f_a and f_p are defined as follows:

$$f_a = \frac{1}{nT_R}\int_t^{t+nT_R} f_I dt \tag{2}$$

$$f_p = \frac{1}{n}\sum_{i=1}^{i=n} \max\{f_I[(i-1)T_R, iT_R]\}\ (i = 1, 2, \cdots, n) \tag{3}$$

where n is the number of wave cycles. The peak value derived from Equation (3) is the average value of the maximum tension in n wave cycles.

The effects of the airbag interval on the cable tension under the conditions of H_R = 0.05 m and G = 0.34 kg/m are shown in Figure 16. The general variation patterns of the average and peak tensions were the same. Under the given wave period and airbag interval, the values of f_p and f_a first increased and then decreased with the increase in L_S/L_W. The maximum values of f_p and f_a were obtained as L_S/L_W = 0.4 in the phase of cable landing. On the other hand, as L_S/L_W increased to 0.64 in the ending phase, the minimum values of f_p and f_a were obtained. As T_R = 1.5 s, f_p and f_a peaked for I_A/λ = 6.5 × 10^{-2}. Additionally, as T_R = 1.5 s and T_R = 2.0 s, for a given value of L_S/L_W, the values of f_p and f_a increased as I_A/λ and the wave period increased. The average values of f_p and f_a for T_R = 2.0 s were increased by 54.4% and 76.5% compared to those for T_R = 1.5 s. For a smaller airbag interval, the average values of f_p and f_a for various wave periods and cable lengths were 0.81 × 10^4 and 0.56 × 10^4. For a larger interval, the average values of f_p and f_a were increased by 24.4% and 29.9%, respectively.

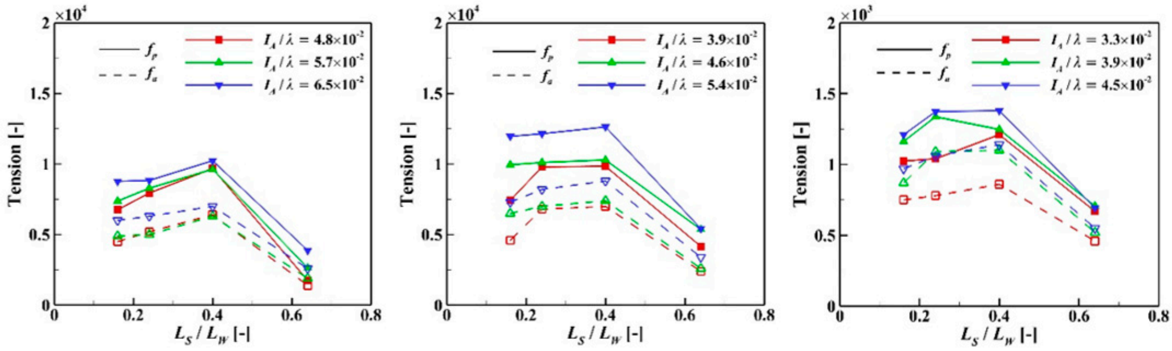

(**a**) (**b**) (**c**)

Figure 16. Effects of the airbag interval on cable tension (H_R = 0.05 m): (**a**) T_R = 1.5 s, (**b**) T_R = 1.75 s, (**c**) T_R = 2.0 s.

For H_R = 0.1 m and G = 0.34 kg/m, the nondimensional cable tensions for various airbag intervals and cable lengths in the water are shown in Figure 17. Similarly, the values of f_p and f_a also decreased as L_S/L_W increased. Compared to the results for H_R = 0.05 m, the average values of f_p and f_a for various wave periods were increased by 77.8%, 41.3%, and 31.2%, and 95.2%, 63.9%, and 32.2%, respectively. The effects of the airbag interval and the incident wave period for a given value of L_S/L_W were reduced significantly. For smaller and larger intervals, the average values of f_p and f_a were 1.29 × 10^4 and 1.35 × 10^4. The average value of f_p for T_R = 2.0 s was larger than that for T_R = 1.5 s by 12.2%.

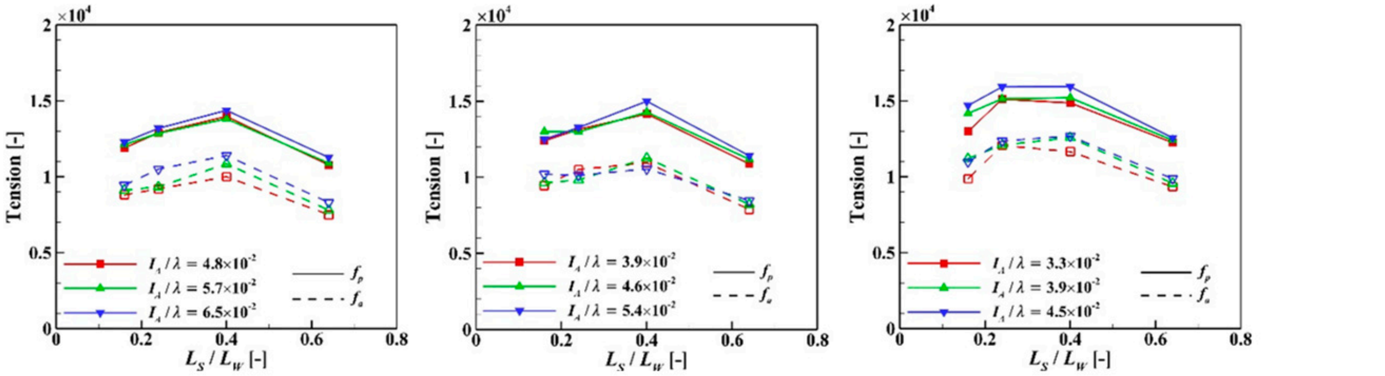

(**a**) (**b**) (**c**)

Figure 17. Effects of the airbag interval on the cable tension (H_R = 0.1 m), (**a**) T_R = 1.5 s, (**b**) T_R = 1.75 s, (**c**) T_R = 2.0 s.

It can be summarized that the values of f_p and f_a both increased as the incident wave height increased. The tensions first increased and then decreased with the increase of the cable length in the water, and the peak values were obtained in the landing phase. For a smaller wave height, the values of f_p and f_a increased with the increase in the airbag interval and the incident wave height, but this was hard to observe for the larger wave height. By comparing with Figure 14, it can be seen that a similar regularity of tension and vertical displacement was expressed in different stages. However, during the ending phase, sufficient bearing force provided by the seabed was the reason for reducing the tension on the cable.

4.4. Effects of Cable Mass on Displacement and Tension

For investigation of the effects of the cable mass, the airbag intervals were adjusted to 17.0 cm, 13.0 cm, and 9.8 cm to ensure the same submerged depths for three typical masses. The vertical displacements for three cable masses under the wave height of H_R = 0.05 m are shown in Figure 18. The relative displacements for various cable masses were all less than 1.0, and all showed peak values at the landing phase. Furthermore, the displacement amplitude decreased as the cable mass increased. For T_R = 1.5 s, the relative displacement amplitudes were 0.72, 0.63, and 0.51, respectively. As the incident wave condition was fixed, an increase in the cable mass caused a reduction of the vertical oscillation of the cable. Similar variation characteristics were also observed for H_R = 0.1 m, as shown in Figure 19.

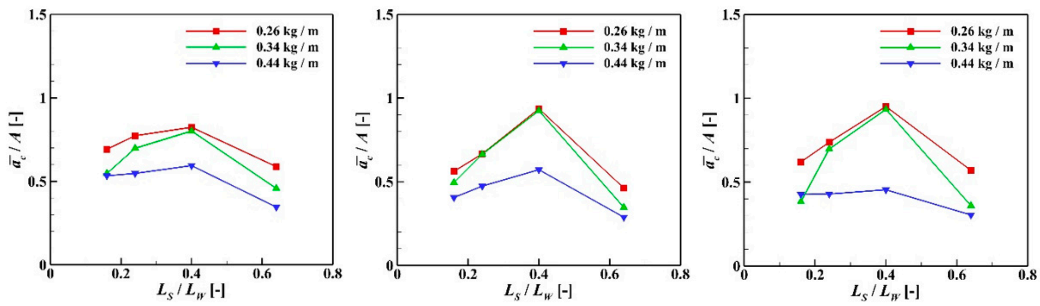

(a) (b) (c)

Figure 18. Effects of the cable mass on cable displacement (H_R = 0.05 m): (**a**) T_R = 1.5 s, (**b**) T_R = 1.75 s, (**c**) T_R = 2.0 s.

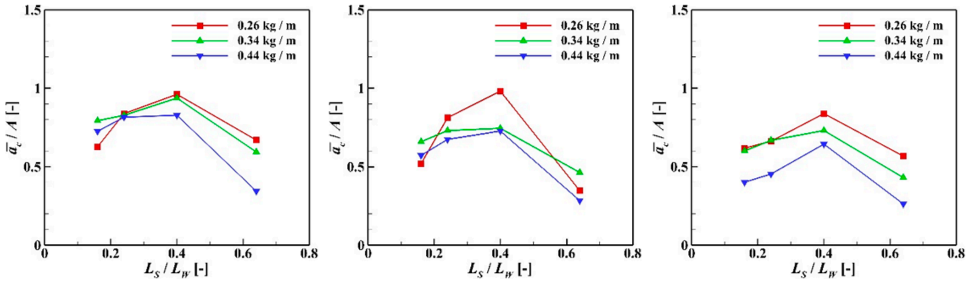

(**a**) (**b**) (**c**)

Figure 19. Effects of the cable mass on cable displacement (H_R = 0.1 m): (**a**) T_R = 1.5 s, (**b**) T_R = 1.75 s, (**c**) T_R = 2.0 s.

The effects of the cable mass on the tension for H_R = 0.05 m are illustrated in Figure 20. The variation trends of f_p and f_a for various cable masses were similar. The peak values were obtained at the landing phase (L_S/L_W = 0.4), and the tensions increased with the increases in the cable mass and the incident wave period. The maximum values of f_p and f_a were obtained for G = 0.44 kg/m. Compared to the average values of f_p and f_a for T_R = 1.5 s, the values for T_R = 2.0 s were increased by 28.6% and 41.6%, respectively. The variation characteristics of the tensions for H_R =0.1 m in Figure 21 were similar to those in Figure 20. The tensions first increased and then decreased as the value of L_S/L_W increased. The f_p and f_a values also showed a significant increase in the average values. All the above results indicate that the vertical displacement amplitudes and the values of f_p and f_a all increased significantly as the cable mass increased, and the maximum values were obtained in the landing phase.

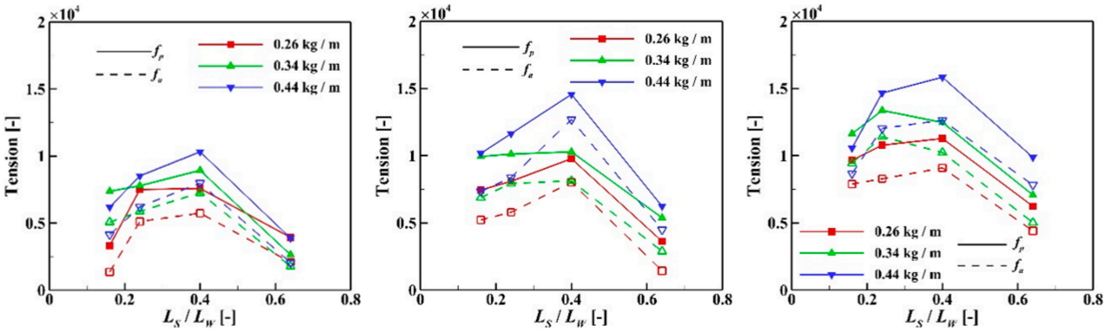

(**a**) (**b**) (**c**)

Figure 20. Effects of the cable mass on the cable tension (H_R = 0.05 m): (**a**) T_R = 1.5 s, (**b**) T_R = 1.75 s, (**c**) T_R = 2.0 s.

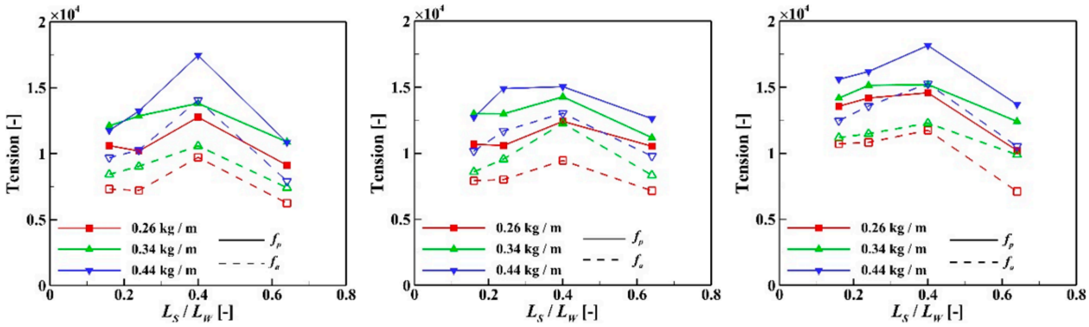

(a) (b) (c)

Figure 21. Effects of the cable mass on the cable tension (H_R = 0.1 m): (**a**) T_R = 1.5 s, (**b**) T_R = 1.75 s, (**c**) T_R = 2.0 s.

5. Conclusions

1. In this study, experiments on landing cables with airbags were conducted in a wave flume, focusing on the cable vertical displacements and tensions during different landing construction phases under regular wave conditions.

2. For the vertical displacement of the cable, the effect of the cable mass increased as the airbag interval increased and the average displacement amplitude decreased. Meanwhile, for a given interval, the displacement amplitude showed a decreasing trend as the incident wave period increased. Under the condition of a smaller wave height, the tensions in the cable both increased with the increase in the incident wave period. Additionally, for a larger wave height, the effects of the airbag interval and the incident wave condition on the tensions were minor. Furthermore, the vertical displacement and tensions both first increased and then decreased as the cable approached the shore. Most values peaked at the landing phase. As the cable mass increased, the vertical displacement amplitude decreased and the tensions increased. These values also peaked at the landing phase. It is suggested to increase the number of airbags used in the landing phase to control the tension and displacement of the cable.

3. In the future, more studies will be conducted to investigate cable hydrodynamic characteristics under real sea conditions, including irregular wave conditions and the coastal stream. Submerged depths in still waters with different airbag intervals will also be studied to provide more valuable information to support the practical construction of cable landings.

Author Contributions: Conceptualization, S.B. and Z.L.; formal analysis, Z.Z.; investigation, S.B. and Z.Y.; data curation, Q.Y. and J.W.; writing—original draft preparation, Z.Z. and Z.L.; writing—review and editing, S.B. and Z.L. All authors have read and agreed to the published version of the manuscript.

Funding: This research received no external funding.

Institutional Review Board Statement: Not applicable.

Informed Consent Statement: Not applicable.

Data Availability Statement: Not applicable.

Acknowledgments: This work was supported by resources provided by the Zhejiang Qiming Electric Power Group Co., Ltd. Submarine Power Cable Engineering Company, with funding from the Research on the Key Technologies of the New Floating Devices for Submarine Cable Landing operation.

Conflicts of Interest: The authors declare no conflict of interest.

References

1. Worzyk, T. *Submarine Power Cables: Design, Installation, Repair, Environmental Aspects*; Springer Science & Business Media: Berlin/Heidelberg, Germany, 2009.
2. Zhang, W.; Zhao, Z.; Tang, Y.; Qu, H. Application of Impressed Current Cathodic Protection in Offshore Oil Platform 161. *Tianjin Sci. Technol.* **2017**, *44*, 55–57. [CrossRef]
3. Chang, H.-C.; Chen, B.-F. Mechanical behavior of submarine cable under coupled tension, torsion and compressive loads. *Ocean Eng.* **2019**, *189*, 106272. [CrossRef]
4. Wang, Z. Technical summary of Marine cable landing construction scheme for offshore wind farm. *Wind Energy* **2019**, *11*, 83–86.
5. Zhang, Z.; Zhang, P.; Ding, Z.; Gong, Y.; Zeng, H.; Liu, Z. The floaters for submarine-cable landing and its engineering applications. *J. Phys. Conf. Ser.* **2021**, *1865*, 032082. [CrossRef]
6. Zajac, E.E. Dynamics and Kinematics of the Laying and Recovery of Submarine Cable. *Bell Syst. Tech. J.* **1957**, *36*, 1129–1207. [CrossRef]
7. Huang, S. Dynamic analysis of three-dimensional marine cables. *Ocean Eng.* **1994**, *21*, 587–605. [CrossRef]
8. Vaz, M.; Patel, M. Transient behaviour of towed marine cables in two dimensions. *Appl. Ocean Res.* **1995**, *17*, 143–153. [CrossRef]
9. Vaz, M.A.; Witz, J.A.; Patel, M.H. Three dimensional transient analysis of the installation of marine cables. *Acta Mech.* **1997**, *124*, 1–26. [CrossRef]
10. Vaz, M.A.; Patel, M. Three-dimensional behaviour of elastic marine cables in sheared currents. *Appl. Ocean Res.* **2000**, *22*, 45–53. [CrossRef]

11. Hover, F.; Grosenbaugh, M.; Triantafyllou, M. Calculation of dynamic motions and tensions in towed underwater cables. *IEEE J. Ocean. Eng.* **1994**, *19*, 449–457. [CrossRef]
12. Wang, Y.; Bian, X.; Zhang, X.; Xie, W. A study on the influence of cable tension on the movement of cable laying ship. In Proceedings of the OCEANS 2010 MTS/IEEE SEATTLE, Seattle, WA, USA, 20–23 September 2010; pp. 1–8.
13. Park, H.; Jung, D.; Koterayama, W. A numerical and experimental study on dynamics of a towed low-tension cable. In Proceedings of the Twelfth International Offshore and Polar Engineering Conference, Kitakyushu, Japan, 26–31 May 2002; OnePetro: Richardson, TX, USA, 2002.
14. Cao, S.; Zhang, J.; Sun, X.; Liang, P. Tension analysis of high voltage submarine cable laying considering bending stiffness. *Taiyangneng Xuebao/Acta Energ. Sol. Sin.* **2019**, *40*, 3009–3016.
15. Jasman, N.A.; Normisyidi, N.A.L.; Hoe, Y.S.; Abidin, A.R.Z.; Haniffah, M.R.M. Numerical Calculation of Two-Dimensional Subsea Cable Tension Problem Using Minimization Approach. *Malays. J. Ind. Appl. Math.* **2019**, *35*, 15–32. [CrossRef]
16. Mamatsopoulos, V.A.; Michailides, C.; Theotokoglou, E.E. An Analysis Tool for the Installation of Submarine Cables in an S-Lay Configuration Including "In and Out of Water" Cable Segments. *J. Mar. Sci. Eng.* **2020**, *8*, 48. [CrossRef]
17. Nagatomi, O.; Nakamura, M.; Koterayama, W. Dynamic simulation and field experiment of submarine cable during laying and recovery. In Proceedings of the Twelfth International Offshore and Polar Engineering Conference, Kitakyushu, Japan, 26–31 May 2002; OnePetro: Richardson, TX, USA, 2002.
18. Prpić, J.; Nabergoj, R. Dynamic tension of marine cables during laying operations in irregular waves. *Int. Shipbuild. Prog.* **2001**, *48*, 149–167.
19. Yang, N.; Jeng, D.-S.; Zhou, X.L. Tension Analysis of Submarine Cables during Laying Operations. *Open Civ. Eng. J.* **2013**, *7*, 282–291. [CrossRef]
20. Feng, Y.; Shang, Q.; Lv, A. Dynamic Finite Element Analysis of Fiber-Optic Composite Submarine Cable Under Wave. *Study Opt. Commun.* **2017**, *4*, 30–34.
21. Ye, Y.-C.; Jiang, X.; Pan, G.; Jiang, W. *Submarine Optical Cable Engineering*; Academic Press: Cambridge, MA, USA, 2018.
22. Zhang, D.; Bai, Y.; Zhao, W.; Zhu, K. Dynamic analysis of submarine cable during the process of laying back to the seabed. *Ships Offshore Struct.* **2020**, *15*, 153–161. [CrossRef]
23. Nexans, Lavrio Syros Interconnector Project. Available online: https://www.nexans.com/business/power-generation-transmission/subsea-interconnectors/Lavrio---Syros.html (accessed on 15 October 2021).